ACS SENSORS

pubs.acs.org/acssensors

Article

Fiber-Tip Shear Force Probe for Single-Cell Adhesion Force Measurements

Mengqiang Zou, Yanping Chen,* Yu Liu, Yiping Wang, and Changrui Liao*

Cite This: *ACS Sens.* 2025, 10, 8874−8884

Read Online

ACCESS | Metrics & More | Article Recommendations | Supporting Information

ABSTRACT: Single-cell adhesion studies play a crucial role in cell biology. Cell adhesion measurement methods, such as atomic force microscopy (AFM) technology, can be used to measure the single-cell adhesion force. However, these methods have many limitations, such as complex operations or the need for labeling. In this study, we proposed a miniature fiber-tip shear force probe (FSFP) that can achieve accurate measurement of the single-cell adhesion force under physiological conditions. A shear force probe structure that facilitates lateral manipulation was designed based on the principles of structural mechanics and fabricated integrally at the end face of a single-mode fiber using femtosecond laser two-photon polymerization technology. The relationship between the FSFP spectral output and the applied force was established, and its microforce sensitivity was obtained to be 2.81 nm/μN, a minimal detectable force is 7.1 nN. The achieved overall measurement range of the device is 69 μN. The adhesion force of MCF-7 breast cancer cells was measured under physiological conditions by using the FSFP. Compared to polymer substrates, the average adhesion force of cells was greater on glass substrates with greater stiffness. The average cell adhesion force value decreased by more than two times after trypsin stimulation. In addition, experiments have shown that cells tend to spread into shuttle shapes on glass substrates with greater stiffness and have a denser actin filaments distribution. To the best of our knowledge, this is the first report on the accurate measurement of the single-cell adhesion force using a miniature all-fiber microforce sensor, which is flexible, fast, and label-free, opening new avenues for single-cell analysis.

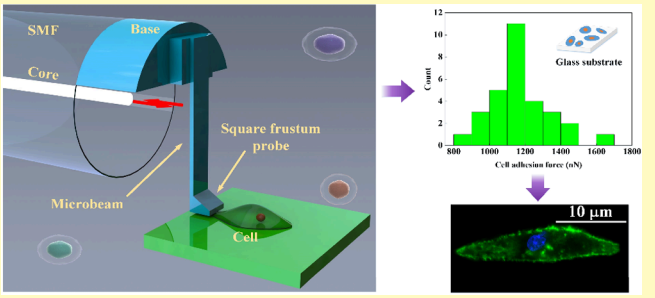

KEYWORDS: *optical fiber sensor, biosensor, two-photon polymerization, cell adhesion, single-cell analysis*

Cell adhesion is critical in a variety of developmental functions, and most cells must adhere to surfaces in their environment to survive.[1,2] Cells spread and form organized actin and complex transmembrane signaling regions after adhering to the substrate, and then the cells begin to express functions such as proliferation, differentiation, and migration.[3,4] The characteristics of cell adhesion not only affect the morphology and function of cells but also are closely related to the occurrence and development of various diseases, such as cancer,[5,6] arthritis,[7] and cardiovascular disease.[8,9] In addition, the adhesion between cells and substrates is closely related to the cell viability. When cell viability is low or death occurs, the number of surface molecular bonds rapidly decreases, resulting in a reduction in the adhesion force of the cells.[10,11] It should also be noted that for different types of cells adhesion kinetics are often characteristic of a given cell type. Cells can actively adhere to a fibronectin-coated surface, forming adhesion complexes and thus having shape characteristics of the given cell type. Moreover, different types of cells bind to different cell adhesion motifs in distinct ratios, depending on their specific integrin receptors and adhesion mechanisms, resulting in differences in adhesion strengths and patterns.[12,13] The study of cell adhesion is a key factor in understanding cell−substrate behavior, and quantifying live cell adhesion forces is essential for understanding cellular physiological processes.

In recent years, research on single-cell adhesion has aroused widespread interest.[14,15] Studies based on cell populations can only give average biological results, which may mask differences between individual cells, and a more precise understanding of the differences between individual cells can help to better understand physiological processes.[16−18] However, it is extremely challenging to realize fast and accurate measurement of the single-cell adhesion force under physiological conditions. Currently, single-cell adhesion force measurements are often performed using robotic fluidic force microscopy (FluidFM),[1] resonant waveguide grating (RWG) biosensor,[12,19] computer controlled micropipette (CCM),[20] microfluidics,[21,22] optical tweezers,[23] and atomic force microscopy (AFM) techniques.[24] Robotic FluidFM allows

Received: August 3, 2025
Revised: November 5, 2025
Accepted: November 10, 2025
Published: November 18, 2025

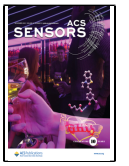

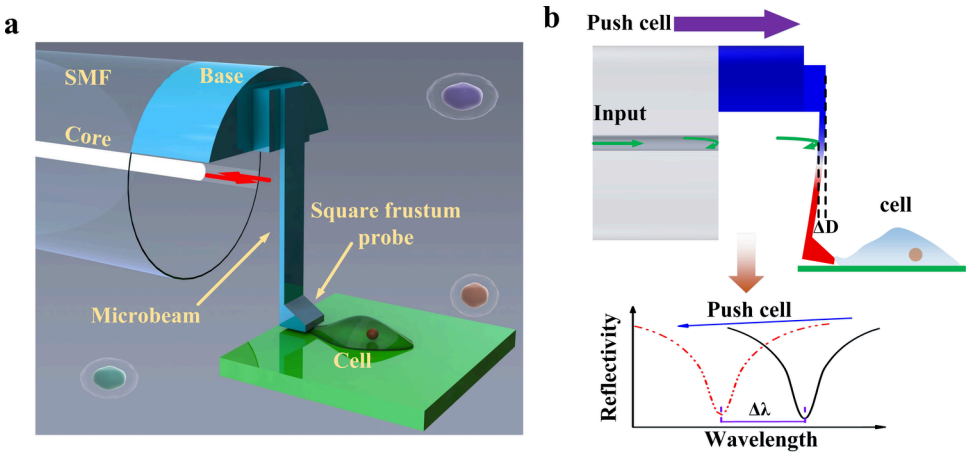

Figure 1. Structure diagram and working principle of FSFP. (a) Schematic structure of FSFP based on a shear force probe. (b) Simulation diagram of the working principle of FSFP.

the disposition or suction of fluids in a femtoliter scale and enables mature adhesion contact measurement in a high-throughput manner, obtaining corresponding force−distance curves and extracting the maximal adhesion force and adhesion energy values. Force calibrated single-cell RWG can measure the local refractive index changes near 150 nm on the sensor surface, thus providing real-time kinetic information about cell adhesion and spreading. CCM technology can measure the adhesion force of surface-attached cells by applying different vacuum levels above the detected cell. The microfluidic technique obtains the adhesion characteristics of cells to the substrate by placing the cells in a laminar flow and applying a controlled fluid shear force to disengage the cells, but the method can only qualitatively assess the adhesion strength of the cells, and a precise adhesion force value cannot be obtained. Optical tweezer technology achieves cell adhesion force by using a highly focused laser beam to capture and manipulate tiny particles such as bacteria or cells, but it is usually only applicable to suspended cells.[25] AFM utilizes a microcantilever to separate the cells from the culture substrate, enabling quantitative adhesion force measurements that are label-free, real-time, and high-resolution.[26−28] Single-cell RWG sensors have a very high throughput and can simultaneously measure thousands of cells. CCM can measure the adhesion of individual cells with relatively high throughput (approximately hundreds of cells within 30 min). The throughput of optical tweezers and AFM is very low with only a few cells per hour. The throughput of Robotic FluidFM is 10 times higher than that of traditional AFM.[19] In 2024, Li et al. measured the adhesion force of HMrSV5 cells based on AFM-based single-cell force spectroscopy and investigated the effect of the fluid environment on single-cell adhesion.[29] However, microcantilevers, the key driving elements of AFMs, generally need to be functionalized and modified before the cells attach. Afterward, the cells are separated from the substrate, and a new microcantilever needs to be replaced for each cell for a new measurement. In this case, replacing and calibrating the microcantilever increase the difficulty of this operation and reduce the efficiency and throughput.[25,30] In addition, traditional AFM has a large volume and complex operation, which greatly limits its flexibility and flux in the application.[31] Therefore, it is urgent to develop a new generation of miniaturized, integrated, and sensitive microforce sensors to achieve flexible, fast, and accurate measurement of the single-cell adhesion force.

Optical fiber sensors have the advantages of small size, flexibility, and biocompatibility.[32−35] However, no reports on the use of all-fiber microforce sensors to measure single-cell adhesion force have been carried out to the best of our knowledge. This may be due to the low force resolution and single shape structure of fiber optic microforce sensors composed of pure silica. To achieve flexible and accurate measurement of cell adhesion force, it is necessary to construct novel fiber optic microforce sensors using new materials and fabricating techniques. Femtosecond laser two-photon polymerization (TPP) is a novel 3D microprinting technology induced by femtosecond laser, which has the advantages of high processing accuracy and flexible processing.[36] TPP technology can integrate micronano functional structures on traditional optical fibers.[37−39] Therefore, the combination of traditional fiber optic and TPP technology has created a new solution for developing miniaturized all-fiber microforce sensors.[40,41]

Herein, we present a compact fiber-tip shear force probe (FSFP) that achieves fast, noninvasive, and accurate measurement of single-cell adhesion force under physiological conditions. Based on the principles of structural mechanics, a shear force probe suitable for lateral operation was designed using the finite element method, and an integrated fabrication of the device was achieved using femtosecond laser TPP technology. The functional relationship between the applied force and the dip wavelength of the FSFP was established, and its microforce sensitivity was obtained to be 2.81 nm/μN. The adhesion force of MCF-7 breast cancer cells was measured with this FSFP. Furthermore, the effects of culture substrate and biological reagent stimulation on single-cell adhesion were investigated. The results indicate that the stiffness of the substrate affects the spreading of cells and the formation of actin and thus further affects the adhesion force of cells. Furthermore, this proposed FSFP can measure the adhesion force of fully adhered cells and has great potential for single-cell activity analysis application.

RESULTS AND DISCUSSION

Sensor Construction and Theoretical Basis. Figure 1a demonstrates a schematic diagram of an FSFP structure integrally printed using femtosecond laser TPP technology.

https://doi.org/10.1021/acssensors.5c02849
ACS Sens. 2025, 10, 8874−8884

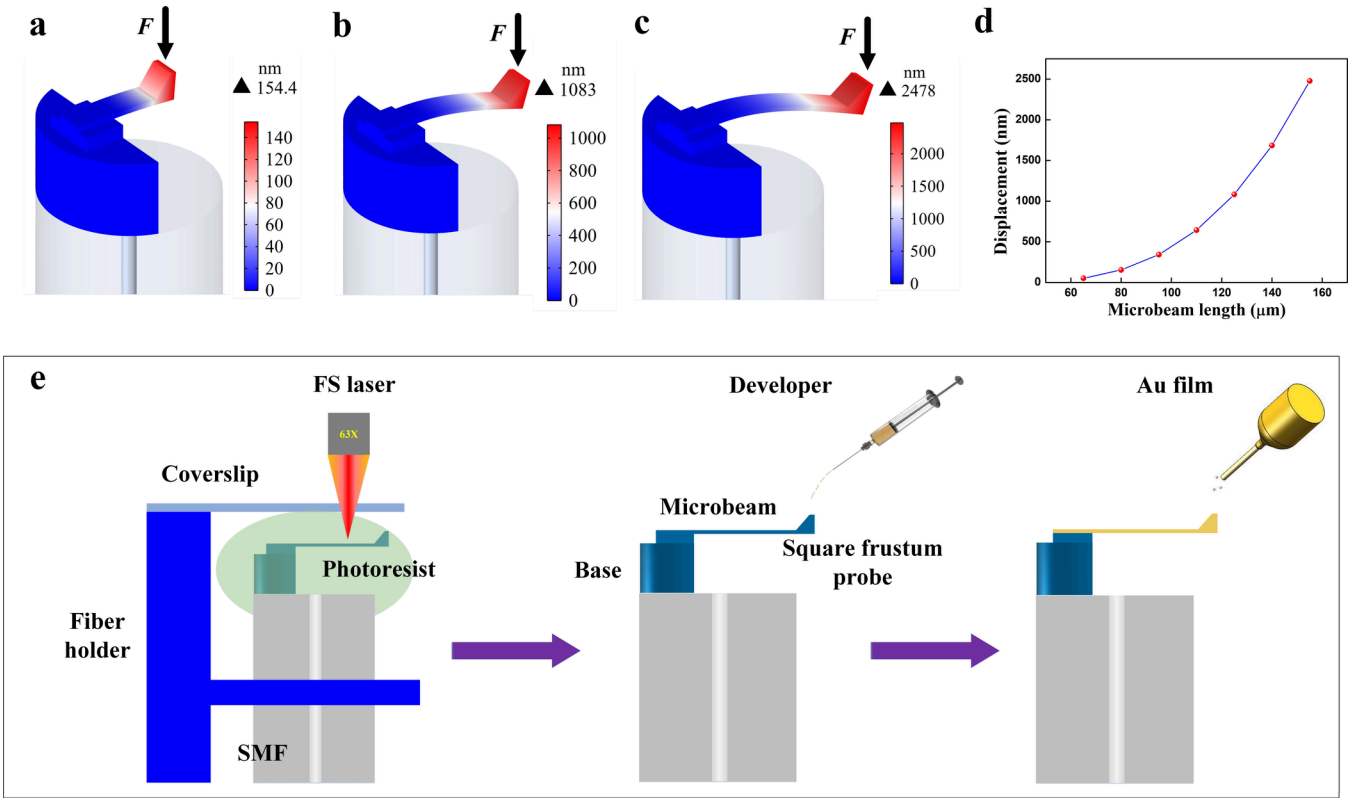

Figure 2. (a–c) Simulation results of bending deformation when the same microforce (1000 nN) was applied to FSFP with different microbeam lengths (80, 125, and 155 μm). (d) Relationship curve between bending deformation and microbeam length. (e) Fabrication process of FSFP.

The structure includes a single-mode fiber (SMF), a base, a microbeam, and a square frustum probe. The base that connects the fiber end face and supports the microbeam was designed as a combination of semicylindrical and rectangular forms to increase the stability of adhesion of the base to the fiber end face and to enhance the robustness of the device. The thickness, width, and length of the microbeam are 3, 20, and 125 μm, respectively. To ensure that the square frustum probe can first touch the target sample once pushing the sample laterally in the horizontal plane, the end of the microbeam was designed to exceed the edge of the fiber end face. A square frustum probe was printed at the end of the microbeam, and the top of the square frustum probe is a rectangular surface with a length of 20 μm and a width of 5 μm. The rectangular surface enables the force surface be larger and more uniform when pushing cells and prevents the probe from puncturing the cell membrane during the pushing process. The combination of base, microbeam, and square frustum probe forms a micro push rod, which is convenient for lateral operation. In addition, to increase the reflectivity of the microbeam surface and improve the biocompatibility of the shear force probe, a gold coating was deposited on the surface of the microbeam and the square frustum probe by using a magnetron sputtering coating instrument.[42,43]

Figure 1b illustrates the working principle of the FSFP. The fiber end face and the surface of the microbeam form a Fabry–Perot cavity. The incident light is reflected at both the fiber end face and the surface of the microbeam, respectively, and multiple beams of reflected light interfere in the core, forming a reflection spectrum. When the FSFP pushes against small objects such as cells, the reaction force of the small objects will cause bending deformation of the microbeam, resulting in a change in the cavity length D of the Fabry–Perot cavity, leading to a shift in the dip wavelength λ of the reflection spectrum. The relationship[44] between the cavity length change (ΔD) and the dip wavelength drift ($\Delta\lambda$) satisfies: $\Delta\lambda/\lambda = \Delta D/D$. Therefore, the force exerted on the FSFP, i.e., the force applied to small objects such as cells, can be obtained by monitoring the dip wavelength of the reflection spectrum.

Construction Simulation and Fabrication. To optimize the structural mechanical properties of the FSFP, a mechanical simulation model of the structure was established using COMSOL Multiphysics finite element software. In the simulation model, the density, Poisson's ratio, and Young's modulus of the shear force probe structural material are set to be 1499 kg/m^3, 0.33, and 2.34 GPa, respectively,[40] while the density, Poisson's ratio, and Young's modulus of the fiber optic material are set to be 2700 kg/m^3, 0.17, and 73 GPa, respectively.[40] To investigate the microforce sensitivity influence of the microbeams length, the lengths of the microbeams were set to be 80, 125, and 155 μm, while all the other geometric parameters are the same. When the same force of 1000 nN is applied to the probe, the bending deformation simulation results of the FSFP are shown in Figures 2a–c. It is clear that under the same force, the maximum bending deformation are 154.4, 1083, and 2478 nm, corresponding to FSFP with different length of 80, 125, and 155 μm, respectively. Thus, the bending deformation increases with the increase of microbeam length, indicating that increasing the microbeam length can improve the microforce sensitivity of the FSFP.

The relationship between the length of the microbeam and the bending deformation under the same force (1000 nN) is concluded and shown in Figure 2d. This indicates that as the

https://doi.org/10.1021/acssensors.5c02849
ACS Sens. 2025, 10, 8874–8884

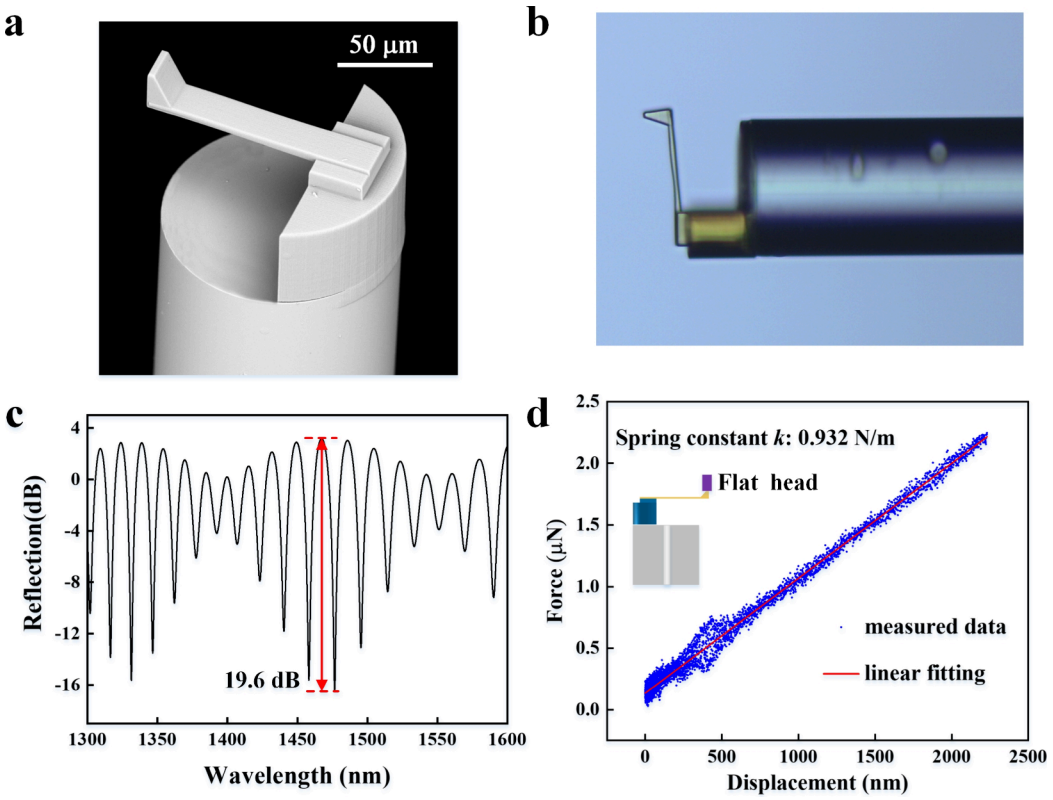

Figure 3. Performance characterization of FSFP. (a) SEM image of the device. (b) Optical microscope image of the device. (c) Reflection spectrum of the device. (d) Elastic properties of the device.

length of the microbeam increases, the bending deformation of the shear force probe increases rapidly, which is consistent with the theory that the bending deformation of the microbeam is proportional to the third power of the length.[45] The FSFP with a longer length microbeam has higher microforce sensitivity. However, excessively long microbeams can also reduce their mechanical strength and robustness, making them susceptible to damage from the surface tension of the developer during the development process.[46] Herein, the length of the microbeam was chosen to be 125 μm by considering the microforce sensitivity, convenience of lateral operation, and mechanical strength.

The integrated device was fabricated by using femtosecond laser TPP technology. As shown in Figure 2e, the fabrication process of the FSFP includes three steps. The first step is to vertically fix an SMF onto a fiber holder and fill the gap between the fiber end face and the coverslip with photoresist. The shear force probe structure designed was then printed in a preset path by focusing the femtosecond laser on the end face of the SMF through a 63x oil-immersion objective (NA = 1.4). The repetition frequency and central wavelength of the femtosecond laser were 200 kHz and 1026 nm, respectively. To improve fabrication efficiency, the output power and scanning speed of the femtosecond laser were set to be 1.8 mW and 800 μm/s, respectively. In the second step, as shown in the middle of Figure 2e, after printing was completed, the fiber was removed from the fiber holder, and the developer solution mixed with acetone and isopropanol (volume ratio of 1:3) was carefully dripped onto the optical fiber end face through a syringe to remove the unpolymerized photoresist. After this step, a shear force probe structure can be achieved. Finally, as shown on the right side of Figure 2e, a gold film with a thickness of ~20 nm was deposited on the surfaces of the microbeam and the square frustum probe to increase the reflectivity of the microbeam surface using a magnetron sputtering coating instrument.

Characterization. The structural morphology, optical properties, and elastic properties of the fabricated FSFP were characterized, as shown in Figure 3. Figure 3a demonstrates the 3D morphology of the device structure captured by using a scanning electron microscope (SEM). It is clear that the shear force probe, which consists of a combination of base, microbeam, and square frustum probe, was completely printed according to the predesign, and the surface was smooth and flat. Even though the length of the microbeam exceeds the edge of the fiber, its overall shape remains straight, with uniform thickness and good parallelism with the fiber end face. The square frustum probe is stably printed at the end of the microbeam. The combination of a semicylinder and a rectangular prism forms a base, which connects and supports the microbeam, and adheres stably to the fiber end face. All these characteristics indicate the flexibility and reliability of using femtosecond laser TPP technology to print shear force probe structures. Figure 3b is a side view of the FSFP obtained using an optical microscope. From this optical microscope images, the core and cladding of the SMF can be clearly observed, and the core is directly opposite to the surface of the microbeam, so that the light exiting from the core was reflected back to the fiber core at both the surface of the microbeam and the fiber end face, resulting in a reflection spectrum. Then, the reflection spectrum of the FSFP, as shown in Figure 3c, was obtained by using a broadband light source and an optical spectrum analyzer. The maximum contrast of the reflection spectrum of the device is over 19.6 dB, and the free spectral

https://doi.org/10.1021/acssensors.5c02849
ACS Sens. 2025, 10, 8874−8884

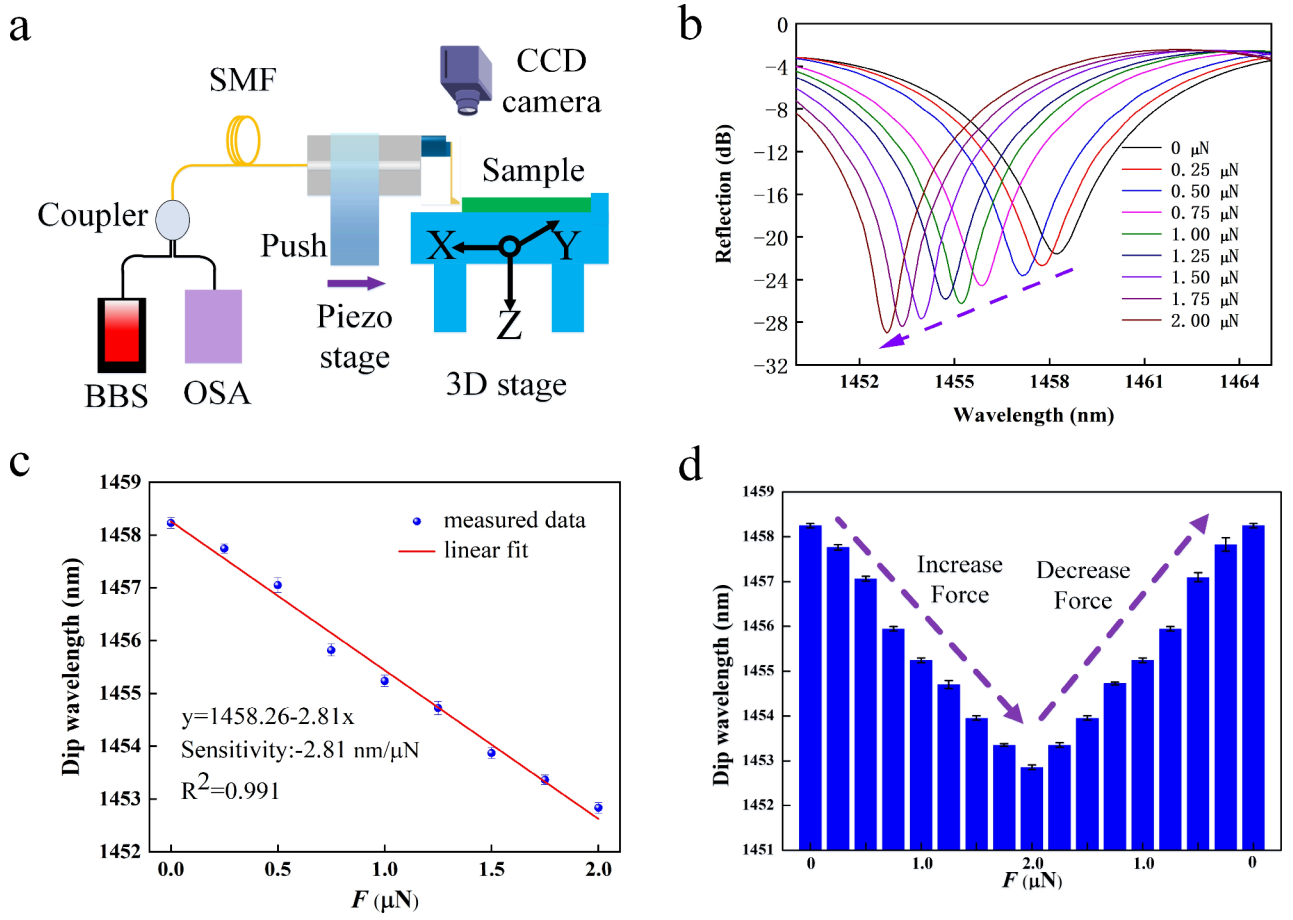

Figure 4. (a) Microforce testing system. (b) Evolution of the reflection spectrum of devices under a microforce. (c) Dip wavelength shift as a function of external force applied to the FSFP. (d) Repeatability testing of dip wavelength under different microforces.

range (FSR) at 1550 nm is about 17.7 nm. This high contrast characteristic of the reflection spectrum lays the foundation for the biomechanical application of FSFP. As shown in the inset in Figure 3d, the elastic properties of the FSFP were tested by using a commercial nanoindenter transducer (Hysitron TriboIndenter TI980, USA) and its matching cylindrical flat indenter. The cylindrical flat head gradually presses down, applying force to the shear force probe to cause a bending deformation of the microbeam. Figure 3d shows the obtained force−deflection curve of the FSFP. It can be seen that there is a linear relationship between force and deflection deformation, and its spring constant k is calculated to be 0.932 N/m by linear fitting of the measured data.[47]

Force Measurement. Prior to single-cell adhesion force measurements using the FSFP, the relationship between the force applied to the FSFP and the output spectrum, i.e., the relationship between the external force and the dip wavelength, must be quantified. To characterize the microforce sensing characteristics of FSFP, a microforce testing system was set up, as shown in Figure 4a. Furthermore, this microforce testing system is used to accurately measure the cells' adhesion force. This microforce testing system includes a broadband light source (BBS, 600−1700 nm), an optical spectrum analyzer (OSA, resolution 0.02 nm, YOKOGAWA, AQ6317C), a 3 dB coupler, a PI piezoelectric displacement stage (Piezo stage, P-631.XCD, stroke 80 μm, resolution 0.1 nm, linear error 0.02%), a 3D stage, and a charge-coupled device (CCD) camera. The 3D stage is used for mounting and fixing the tested samples and adjusting the height of the samples. The CCD camera is used for real-time observation of the test process. To minimize the impact of environmental vibration and noise, the entire system was mounted on a vibration isolation platform (Newport, S-2000A-116). In addition, to reduce the temperature and humidity fluctuation effect on testing, the microforce testing system is located in a constant temperature and humidity ultra clean room. The FSFP is fixed on a high-precision PI piezoelectric displacement stage and is driven by the PI piezoelectric displacement stage for push testing. The reflection spectrum of the FSFP is carefully tracked and demodulated by the aforementioned optical signal demodulation system aforementioned.

To measure the adhesion characteristics of cells under physiological conditions, the microforce characteristics of the FSFP were measured in phosphate-buffered saline (PBS). The FSFP was driven to press against a hard metal substrate by a PI piezoelectric displacement stage. The microbeam undergoes a bending deformation, and the deflection d_c generated by the microbeam is equal to the displacement d_p of the PI piezoelectric displacement stage. Then, the force acting on the FSFP can be calculated[40,48] by $F = kd_c$. Figure 4b shows the evolution of the reflection spectrum when the FSFP gradually pressed toward the hard metal substrate in a step size of 268.2 nm. According to $F = kd_c$, the microforce exerted on the FSFP at each step is calculated to be 0.25 μN. As the purple dashed arrow shows, as the external force gradually increases from 0 to 2 μN, the reflection spectrum of the FSFP shifts toward the

https://doi.org/10.1021/acssensors.5c02849
ACS Sens. 2025, 10, 8874−8884

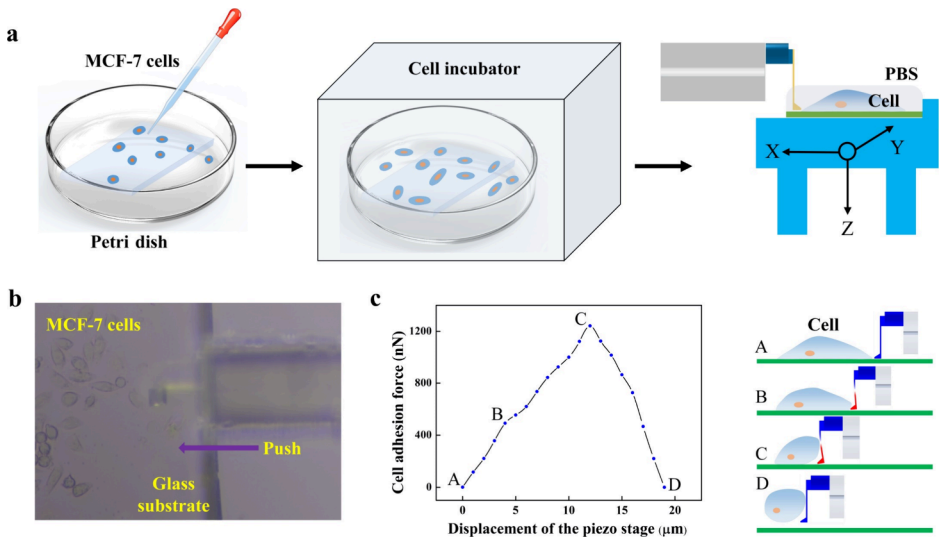

Figure 5. (a) MCF-7 breast cancer cell culture and measurement preparation. (b) Microscopic observation of MCF-7 breast cancer cells pushed using a FSFP. (c) Schematic diagram of push MCF-7 breast cancer cells and a curve of the relationship between the force applied and the propulsive displacement.

short-wave direction, i.e., blue shift, with wavelength shift of ∼5.4 nm, indicating that the prepared FSFP can work stably in the liquid environment. Figure 4c shows the dip wavelength change with external forces, extracted from Figure 4b. A microforce sensitivity of −2.81 nm/μN is obtained by linearly fitting, and the matching degree of the fitting is as high as 0.991. The minimal detectable force can be obtained by the ratio of the resolution of the optical spectrum analyzer that used to the microforce sensitivity.[49] The minimal detectable force of the FSFP is 7.1 nN within the limited 0.02 nm resolution of the optical spectrum analyzer (OSA, YOKOGA-WA, and AQ6317C). Experimentally, the obtained overall measurement range of the device is 69 μN.

To investigate the repeatability and stability of the FSFP force response, three cycle repeatability experiments were conducted. During the measurement, the external force was first increased from 0 to 2 μN and then gradually decreased from 2 to 0 μN, the same steps of 0.25 μN were adopted for both the increasing and decreasing forces. Figure 4d shows the dip wavelength variation during the repeatability test as the different external forces were applied to the FSFP. The results show that the dip wavelength response to the external force is relatively stable and has good repeatability as the external force increased or decreased.

Cell Adhesion Measurement. The characterization of breast cancer cell adhesion will help to understand the potential molecular events that lead to tumor proliferation and can reflect the potential of tumor to malignant development.[50,51] To perform single-cell adhesion force measurements using the proposed FSFP, MCF-7 breast cancer cells were cultured, as shown in Figure 5a. First, a rectangular glass substrate (20 mm × 40 mm × 0.2 mm) was placed in a cell culture dish. The dish was sterilized by placing it in a UV environment, and then MCF-7 breast cancer cells were inoculated into the dish. Then, the culture dish was placed in a cell culture incubator for incubation. Finally, as shown on the right side of Figure 5a, after 24 h of cultivation, the glass substrate in the culture dish was taken out and fixed on the 3D stage of the microforce testing system, and PBS cell buffer was dropped onto the glass substrate to ensure environmental stability of the cells during the testing process.

A real-time observation of the MCF-7 breast cancer cells pushed laterally by FSFP was obtained by the CCD camera, as shown in Figure 5b. It is clear that MCF-7 breast cancer cells grow well on the glass substrate, and most of the cancer cells grow individually in a shuttle shape. Large and stable focal adhesive plaques are formed between cancer cells and the glass substrate, which stabilize the adherence of the cancer cells to the wall. In addition, the relative position of the shear force probe and the cancer cell can be clearly observed in Figure 5b, and in this case, the FSFP can be controlled to achieve accurate measurement of the adhesion force of different MCF-7 breast cancer cells.

The FSFP gradually pushes MCF-7 breast cancer cells through carefully controlling the PI piezoelectric displacement stage. Due to the cell adhesion force, the microbeam will undergo bending and deformation in the process of pushing the cancer cells. Thus, the reflection spectrum formed by the microbeam drifts and the magnitude of the force can be obtained by monitoring the dip wavelengths of its reflection spectrum. Figure 5c demonstrates the relationship between the force applied to FSFP and the pushing displacement. The pushing displacement was recorded only when the shear force probe gradually moved toward and contacts the cancer cells, and the first contact point is denoted as point A, corresponding to the schematic diagram A on the right side of Figure 5c. Then, the cancer cells began to deform under the lateral load of the shear force probe. Simultaneously, the shear force probe suffers a reactive force; thus, the microbeam deforms, corresponding to schematic diagram B on the right side of Figure 5c. As the displacement increases, the deformation of cancer cells gradually increases, and the force acting on the FSFP also increases. It is observed that as the shear force probe continues to move, the force gradually reaches to its maximum value and then decreases. Herein, the maximum force value is obtained to be 1239.5 nN, and this maximum force is defined as the adhesion force of a single cell,[10] corresponding to the C diagram on the right side of Figure 5c. From this moment on, cancer cells begin to separate from the glass substrate. As the

https://doi.org/10.1021/acssensors.5c02849
ACS Sens. 2025, 10, 8874−8884

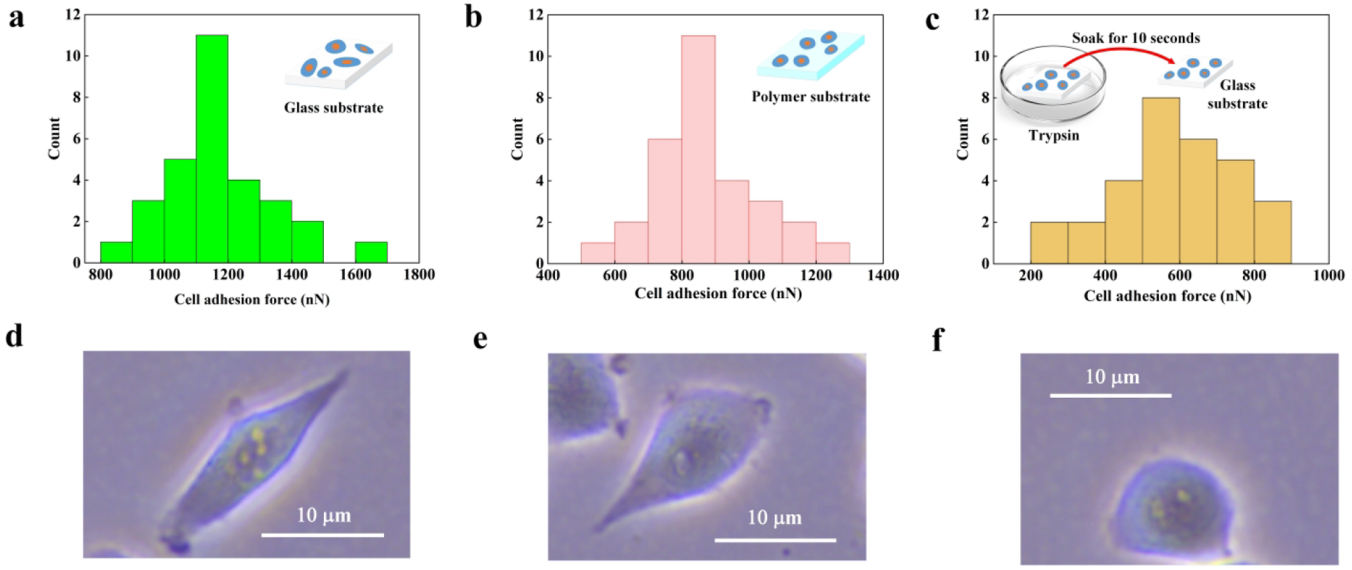

Figure 6. (a) Statistical graph of adhesion force measured on a glass substrate. (b) Statistical graph of adhesion force measured on the polymer substrate. (c) Statistical graph of adhesion force after trypsin stimulation. Panels (d) and (e) are typical optical microscopic images of MCF-7 breast cancer cells on the glass substrate and polymer substrate, respectively. (f) Typical optical microscopy image of cancer cells soaked in trypsin for 10 s.

displacement continues to increase, the degree of separation between cancer cells and the glass substrate increases, and the force acting on the FSFP decreases. Finally, the cancer cells were completely separated from the glass substrate, breaking the molecular bonds between the cancer cells and the glass substrate. At this time, the FSFP is no longer subjected to the reaction force of cancer cells, and the bending deformation of the microbeam disappears, corresponding to the schematic diagram D on the right side of Figure 5c. In addition, after the test, it was found that the morphology of the cancer cells changed from a shuttle shape to a spherical shape after they were detached from the glass substrate from the adherent state while maintaining good activity. Furthermore, this experiment test indicates that the proposed FSFP can achieve fast, noninvasive, and accurate measurement of single-cell adhesion force under physiological conditions.

Cells can sense external environment changes through transmembrane proteins, which in turn affect physiological characteristics such as cell growth, proliferation, and migration.[52] In addition, the culture substrate of cells not only provides physical support but also can affect the cell behavior through its mechanical properties, such as stiffness.[53] To investigate the effect of the culture environment on single-cell adhesion, the adhesion force values of single cells under different culture substrates and bioreagent stimulation were measured using the FSFP. As shown in the cell culture method in Figure 5a, MCF-7 breast cancer cells were inoculated on the glass substrate (Young's modulus of 73 GPa) and the polymer substrate (Young's modulus of 2.34 GPa) under the same experimental conditions, and adhesion force values of 30 single cells were obtained. Figure 6a,b shows the statistical graphs of the adhesion force measured on glass substrates and polymer substrates, respectively. It was found that cancer cells cultured on the same substrates has different adhesion force values. This is mainly because single cells are extremely complex systems with individual variability, and even under the same culture conditions, their physiological characteristics may vary. The maximum value of single cells adhesion on the glass substrate was measured to be 1625.2 nN, and the average value was 1170.3 nN. Meanwhile, the maximum value of single cells adhesion on the polymer substrate was 1211.4 nN, and the average value was 862.1 nN. Thus, it is verified that the MCF-7 breast cancer cells cultured on the glass substrate had a stronger overall adhesion, i.e., it requires a higher shear force to separated cells from the glass substrate. This may be mainly because the stiffness of the substrate affects behaviors such as cell spreading, adhesion plaque formation, and differentiation.[54,55]

To investigate the effect of biological reagent stimulation on single-cell adhesion, as shown in the inset in Figure 6c, cancer cells cultured on a glass substrate for 24 h were soaked in trypsin for 10 s before being taken out. The adhesion force was measured using the FSFP. Figure 6c demonstrates a statistical graph of the adhesion force values of 30 cancer cells measured. The maximum value of single-cell adhesion force is 831.5 nN, and the average value is 565.8 nN. Compared with the results shown in Figure 6a, the adhesion force of single cells has a significant reduction after trypsin stimulation, and the average adhesion force value decreased by more than twice. The reason may be that the adhesion force of a single cell is closely related to the number of molecular bonds,[10] and trypsin stimulation breaks the molecular bonds between the single cells and the substrate.

Figures 6d and 6e are typical optical microscopy images of MCF-7 breast cancer cells on glass and polymer substrates, respectively. It can be seen that on the substrate with larger stiffness, the cancer cells tend to spread into a shuttle shape and has a larger contact area. Also, a larger contact area can help form large and stable focal adhesive plaques with a larger number of molecular bonds formed with the substrate, resulting in larger adhesion. In contrast, on the surface of the substrate with lower stiffness, cancer cells are more inclined to grow into elliptical or spherical with smaller contact areas, resulting in a smaller adhesion force. Figure 6f shows the optical microscope image of cancer cells soaked in trypsin for 10 s. Trypsin can digest the adhesive proteins produced by

https://doi.org/10.1021/acssensors.5c02849
ACS Sens. 2025, 10, 8874−8884

cells, breaking the molecular bonds between single cells and the substrate. Cancer cells are approximately spherical, and the adhesion force rapidly decreases, which agrees well with the measurement results in Figure 6c.

Figure 7a,b illustrates the principle of adhesion between MCF-7 breast cancer cells and the substrate. At the initial stage

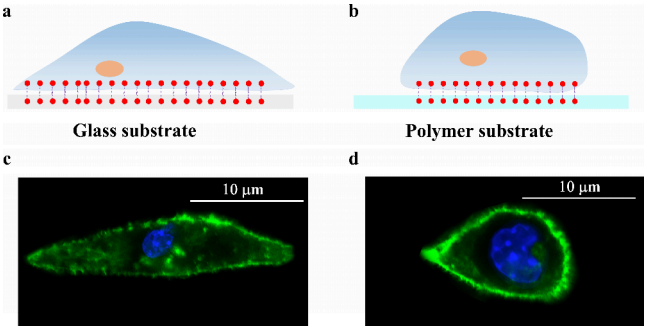

Figure 7. (a) Schematic diagram of the principle of adhesion of MCF-7 breast cancer cells to glass substrates. (b) Schematic diagram of the principle of adhesion of MCF-7 breast cancer cells to polymer substrates. (c) Typical confocal image of MCF-7 breast cancer cells on glass substrates. (d) Typical confocal image of MCF-7 breast cancer cells on polymer substrates.

of adhesion, adhesion molecules such as integrins and cadherins on the cancer cells form adhesion sites and start to attach to the substrate.[1,28] Subsequently, the cells spread on the substrate surface and formed an organized actin cytoskeleton. Finally, adhesion molecules are connected to both the substrate and the cytoskeleton, forming stable molecular bonds links.[56] The adhesion force of cancer cells is the sum of all of the forces generated by all molecular bonds. Typical confocal images of MCF-7 breast cancer cells on the glass substrate and polymer substrate were obtained by a confocal microscope, as shown in Figure 7c,d. The blue color represents the cell nucleus, and the green color represents the actin cytoskeleton. It is clear that the actin filaments of the cancer cells on the polymer substrate are mainly distributed around the cells with only a little inside. However, on the glass substrate, actin filaments are densely distributed both around and inside the cancer cells, and cancer cells are distributed with a denser actin cytoskeleton, which generates traction forces on the substrate and enhances focal adhesion.[57]

Table S1 compares the performance of different cell adhesion measurement techniques. Single-cell RWG biosensors can simultaneously measure thousands of cells, with force resolution force at the nN level,[1,58] but it needs to be calibrated by robotic FluidFM to accurately quantify the force value. Robotic FluidFM, CCM, and AFM systems are all capable of single-cell measurements. Robotic FluidFM can measure approximately 20 cells within 1 h,[19,59] and CCM can measure hundreds of cells within 30 min.[20,60] The throughput of AFM is very low and only a few cells can be measured within 1 h.[29,61] The force resolutions of robotic FluidFM and CCM are both at the nN level, while the force resolution of AFM can reach the pN level. One unique feature of the CCM method is that after the adhesion force measurement individual cells can be isolated for further study. Traction force microscopy (TFM) can be used to quantify the adhesion force exerted by cells throughout the entire cell cycle. However, the throughput of TFM is relatively low, and it can only measure approximately 50 cells within several hours.[62,63] Optical tweezers typically manipulate a cell within 15 min, and the force resolution can reach 0.1 pN. However, lasers may cause damage to cells. The proposed method based on FSFP can directly measure single-cell adhesion force with relatively high throughput, measuring hundreds of cells within half an hour. FSFP can measure the adhesion force of fully adhered cells with a force resolution at the nN level. Moreover, FSFP can achieve noninvasive measurement and analysis of single cells.

CONCLUSIONS

In conclusion, we developed a new method for simple, fast, and noninvasive measurement of single-cell adhesion force based on the proposed FSFP. First, a shear force probe structure that takes into account microforce sensitivity and lateral operation convenience was designed by combining mechanical structure optimization algorithms. Then, the FSFP was integrally fabricated by the femtosecond laser TPP technique, with a microforce sensitivity of up to 2.81 nm/μN, and has excellent mechanical stability and repeatability. Accurate measurement of the single-cell adhesion force under physiological conditions was achieved using the FSFP, and the individual variability in single-cell adhesion was verified. Furthermore, the effect of the culture environment on the adhesion force of MCF-7 breast cancer cells was investigated, and the mechanism of cell adhesion on the substrate was analyzed. It was found that the stiffness of the culture substrate can affect cell spreading, actin formation, and the number of molecular bonds, thus affecting cell adhesion. In addition, the stimulation of biological reagents such as trypsin can break molecular bonds on the cell surface and thus reduce the cell adhesion force. The new FSFP platform is flexible and efficient, without the need for cumbersome cell fixation steps, and can measure the adhesion force of fully adhered cells, which may create new biomedical applications that cannot be achieved by current commercial AFM. It is worth noting that the FSFP is also suitable for measuring lateral forces of various micronano materials and has great potential in biomechanical and material measurement applications.

MATERIALS AND METHODS

Cell Culture. The MCF-7 breast cancer cells (HTB-22, American Type Culture Collection) were cultured in Dulbecco's Modified Eagle's Medium (DMEM, Gibco, USA). An appropriate amount of DMEM cell culture medium (Gibco, USA) containing 10% fetal bovine serum (Gibco, USA), 100 units/mL penicillin, and streptomycin (Gibco, USA) was added to the culture dish. Cells were incubated in a humidified atmosphere at a temperature of 37 °C and 5% CO_2.

Cell Confocal Imaging. Cancer cells cultured for 24 h were taken out of the cell culture incubator and washed with PBS, after which the cells were fixed with 4% paraformaldehyde for 10 min, and washed with PBS after completion of fixation. Then, 0.1% Triton X-100 (Sigma-Aldrich) was added to permeabilize the cells for 10 min, and after permeabilization was completed, the cells were again washed with PBS. Afterward the cells were treated with 1% BSA occlusion for 1 h, labeled with primary antibody (α Tubulin mouse monoclonal antibody) for 3 h, and then washed with PBS. Secondary antibody (Alexa Fluor 647) was then added for 45 min for labeling and washed again using PBS. Then, DAPI (4′,6-diamidino-2-phenylindole) was added and incubated for 20 min to label the nuclei, followed by washing with PBS. Afterward, Alexa Fluor 488 phalloidin (Gibco, Invitrogen Corporation, Melbourne, Australia) was added and incubated for 30 min to label actin filament network (F-actin). After labeling was completed, the cells were rinsed three times with

https://doi.org/10.1021/acssensors.5c02849
ACS Sens. 2025, 10, 8874−8884

PBS and finally imaged by confocal laser microscopy (Zeiss LSM 880).

■ ASSOCIATED CONTENT

Supporting Information

The Supporting Information is available free of charge at https://pubs.acs.org/doi/10.1021/acssensors.5c02849.

Simulation of the influence of microbeam thickness and width on microforce sensitivity, details of temperature cross-interference experiments in FSFP, and performance comparison of different cell adhesion measurement techniques (PDF)

■ AUTHOR INFORMATION

Corresponding Authors

Yanping Chen − *Chongqing Key Laboratory of Autonomous Navigation and Microsystems, Chongqing Engineering Research Center of Intelligent Sensing Technology and Microsystem, School of Electronic Science and Engineering, Chongqing University of Posts and Telecommunications, Chongqing 400065, China;* orcid.org/0009-0004-0810-8937; Email: chenyp@cqupt.edu.cn

Changrui Liao − *Shenzhen Key Laboratory of Ultrafast Laser Micro/Nano Manufacturing, Key Laboratory of Optoelectronic Devices and Systems of Ministry of Education and Guangdong Province, College of Physics and Optoelectronic Engineering and Guangdong and Hong Kong Joint Research Centre for Optical Fiber Sensors, Shenzhen University, Shenzhen 518060, China;* orcid.org/0000-0003-3669-5054; Email: cliao@szu.edu.cn

Authors

Mengqiang Zou − *Chongqing Key Laboratory of Autonomous Navigation and Microsystems, Chongqing Engineering Research Center of Intelligent Sensing Technology and Microsystem, School of Electronic Science and Engineering, Chongqing University of Posts and Telecommunications, Chongqing 400065, China;* orcid.org/0009-0002-9845-0300

Yu Liu − *Chongqing Key Laboratory of Autonomous Navigation and Microsystems, Chongqing Engineering Research Center of Intelligent Sensing Technology and Microsystem, School of Electronic Science and Engineering, Chongqing University of Posts and Telecommunications, Chongqing 400065, China*

Yiping Wang − *Shenzhen Key Laboratory of Ultrafast Laser Micro/Nano Manufacturing, Key Laboratory of Optoelectronic Devices and Systems of Ministry of Education and Guangdong Province, College of Physics and Optoelectronic Engineering and Guangdong and Hong Kong Joint Research Centre for Optical Fiber Sensors, Shenzhen University, Shenzhen 518060, China*

Complete contact information is available at: https://pubs.acs.org/10.1021/acssensors.5c02849

Author Contributions

M.Z. and Y.C. jointly conceived the idea. M.Z. fabricated the fiber-tip shear force probe, built the experimental setup, and carried out the experiments. Y.L., C.L., and Y.W. assisted with the theory. M.Z. and Y.C. analyzed the data and wrote the manuscript. All authors have given approval to the final version of the manuscript.

Funding

This work was supported by the National Natural Science Foundation of China (grant nos. 62405040, 62305039, and T2421003), the Natural Science Foundation of Chongqing (grant nos. CSTB2023NSCQ-LMX0028, CSTB2023NSCQ-MSX0568, and CSTB2022NSCQ-LZX0050), the Science and Technology Research Program of Chongqing Municipal Education Commission (grant no. KJQN202400606), the China Postdoctoral Science Foundation (grant no. 2025M770851), and the Chongqing Postdoctoral Research Project Special Funding (grant nos. 2024CQBSHTB3070 and 2024CQBSHTB3088).

Notes

The authors declare no competing financial interest.

■ REFERENCES

(1) Sztilkovics, M.; Gerecsei, T.; Peter, B.; Saftics, A.; Kurunczi, S.; Szekacs, I.; Szabo, B.; Horvath, R. Single-cell adhesion force kinetics of cell populations from combined label-free optical biosensor and robotic fluidic force microscopy. *Sci. Rep.* **2020**, *10* (1), 61.

(2) Yang, D.; Liu, X.; Ma, J.; Cui, B.; Wang, Y.; Xu, J.; Zhang, Y.; Ding, H.; Wang, D.; Liu, Q.; Zhang, F. Probing Single-Cell Adhesion Kinetics and Nanomechanical Force with Surface Plasmon Resonance Imaging. *ACS Nano* **2025**, *19* (2), 2651−2664.

(3) Dibus, M.; Joshi, O.; Ivaska, J. Novel tools to study cell-ECM interactions, cell adhesion dynamics and migration. *Curr. Opin. Cell Biol.* **2024**, *88*, No. 102355.

(4) Engler, A. J.; Sen, S.; Sweeney, H. L.; Discher, D. E. Matrix Elasticity Directs Stem Cell Lineage Specification - ScienceDirect. *Cell* **2006**, *126* (4), 677−689.

(5) Guo, Q.; Li, L.; Gao, G.; Liu, R.; Einaga, Y.; Zhi, J. Nanodiamonds Inhibit Cancer Cell Migration by Strengthening Cell Adhesion: Implications for Cancer Treatment. *ACS Appl. Mater. Interfaces* **2021**, *13* (8), 9620−9629.

(6) Burčík, D.; Macko, J.; Podrojková, N.; Demeterová, J.; Stano, M.; Oriňak, A. Role of Cell Adhesion in Cancer Metastasis Formation: A Review. *ACS Omega* **2025**, *10* (6), 5193−5213.

(7) Ma, L.; Wu, H.; Cao, J.; Zhang, N.; Li, Y.; Zheng, J.; Jiang, X.; Gao, J. Mesenchymal Stem Cell-Based Biomimetic Liposome for Targeted Treatment of Rheumatoid Arthritis. *ACS Appl. Mater. Interfaces* **2024**, *16* (36), 47206.

(8) Montecillo, J.; Pirker, T.; Pemberton, C.; Chew-Harris, J. Chapter Two - suPAR in cardiovascular disease. *Adv. Clin. Chem.* **2024**, *121*, 89.

(9) Li, H.; Zhang, F.; Wang, D.; Luo, S.; Ding, Z.; Bao, H.; Zhang, S.; Fan, C.; Ji, W.; Wang, S. Specific Cell Adhesion at Nano-Biointerfaces: Synergistic Effect of Topographical Matching and Molecular Recognition. *Nano Lett.* **2025**, *25* (17), 7097−7106.

(10) Shen, Y.; Nakajima, M.; Kojima, S.; Homma, M.; Kojima, M.; Fukuda, T. Single cell adhesion force measurement for cell viability identification using an AFM cantilever-based micro putter. *Measurement Science & Technology* **2011**, *22* (11), 115802.

(11) Bhattacharyya, S.; Mote, R. D.; Freimer, J. W.; Tiwari, M.; Bansi Singh, S.; Arumugam, S.; Narayana, Y. V.; Rajan, R.; Subramanyam, D. Cell-cell adhesions in embryonic stem cells regulate the stability and transcriptional activity of β-catenin. *FEBS Lett.* **2022**, *596* (13), 1647−1660.

(12) Beres, B.; Kovacs, K. D.; Kanyo, N.; Peter, B.; Szekacs, I.; Horvath, R. Label-Free Single-Cell Cancer Classification from the Spatial Distribution of Adhesion Contact Kinetics. *ACS Sens.* **2024**, *9* (11), 5815−5827.

(13) Obara, M.; Sakuma, T.; Fujikawa, K. The third type III module of human fibronectin mediates cell adhesion and migration. *J. Biochem.* **2010**, *147* (3), 327−335.

(14) Khalili, A.; Ahmad, M. A Review of Cell Adhesion Studies for Biomedical and Biological Applications. *Int. J. Mol. Sci.* **2015**, *16* (8), 18149−18184.

(15) Tejeda-Muoz, N.; Mei, K. C. Wnt signaling in cell adhesion, development, and colon cancer. *IUBMB Life* **2024**, *76* (7), 383−396.
(16) Li, M. Harnessing atomic force microscopy-based single-cell analysis to advance physical oncology. *Microsc. Res. Tech.* **2024**, *87* (4), 631.
(17) Fu, Y.; Lin, S.; Wang, X. H. Whispering Gallery Mode Micro/Nanolasers for Intracellular Probing at Single Cell Resolution. *ACS Sens.* **2024**, *9* (11), 5683−5698.
(18) Zhong, Q.; Huang, X.; Zhang, R.; Zhang, K.; Liu, B. Optical sensing strategies for probing single-cell secretion. *ACS Sens.* **2022**, *7* (7), 1779−1790.
(19) Ungai-Salánki, R.; Haty, E.; Gerecsei, T.; Francz, B.; Béres, B.; Sztilkovics, M.; Székács, I.; Szabó, B.; Horvath, R. Single-cell adhesion strength and contact density drops in the M phase of cancer cells. *Sci. Rep.* **2021**, *11* (1), 18500.
(20) Salánki, R.; Hős, C.; Orgovan, N.; Péter, B.; Sándor, N.; Bajtay, Z.; Erdei, A.; Horvath, R.; Szabó, B. Single cell adhesion assay using computer controlled micropipette. *PLoS One* **2014**, *9* (10), No. e111450.
(21) Mutlu, B. R.; Dubash, T.; Dietsche, C.; Mishra, A.; Ozbey, A.; Keim, K.; Edd, J. F.; Haber, D. A.; Maheswaran, S.; Toner, M. In-flow measurement of cell−cell adhesion using oscillatory inertial microfluidics. *Lab Chip* **2020**, *20* (9), 1612−1620.
(22) Wei, M.; Zhang, F.; Zhang, R.; Lin, J. M.; Yang, N. High-Throughput Characterization of Cell Adhesion Strength Using Long-Channel Constriction-Based Microfluidics. *ACS Sens.* **2021**, *6* (8), 2838−2844.
(23) Hardiman, W.; Clark, M.; Friel, C.; Huett, A.; Perez-Cota, F.; Setchfield, K.; Wright, A. J.; Tassieri, M. Living cells as a biological analog of optical tweezers − a non-invasive microrheology approach. *Acta Biomater.* **2023**, *166*, 317−325.
(24) Nishida, K.; Anada, T.; Kobayashi, S.; Ueda, T.; Tanaka, M. Effect of bound water content on cell adhesion strength to water-insoluble polymers. *Acta Biomater.* **2021**, *134*, 313−324.
(25) Zanetti, M.; Chen, S. N.; Conti, M.; Taylor, M. R. G.; Sbaizero, O.; Mestroni, L.; Lazzarino, M. Microfabricated cantilevers for parallelized cell-cell adhesion measurements. *Eur. Biophys. J.* **2022**, *51* (2), 147−156.
(26) Viljoen, A.; Mathelié-Guinlet, M.; Ray, A.; Strohmeyer, N.; Jin Oh, Y.; Hinterdorfer, P.; Müller, D. J.; Alsteens, D.; Dufrêne, Y. F. Force spectroscopy of single cells using atomic force microscopy. *Nat. Rev. Methods Primers* **2021**, *1* (1), 63.
(27) Dufrêne, Y. F. Sticky microbes: Forces in microbial cell adhesion. *Trends Microbiol.* **2015**, *23* (6), 376−382.
(28) Nguyen, T. D.; Gu, Y. T. Investigation of Cell-Substrate Adhesion Properties of Living Chondrocyte by Measuring Adhesive Shear Force and Detachment Using AFM and Inverse FEA. *Sci. Rep.* **2016**, *6*, 38059.
(29) Wei, J.; Yang, Y.; Li, M. Single-cell force spectroscopy of fluid flow-tuned cell adhesion for diBecting hemodynamics in tumor metastasis. *Nanoscale* **2023**, *16* (1), 360−372.
(30) Nagy, Á. G.; Kanyó, N.; Vörös, A.; Székács, I.; Bonyár, A.; Horvath, R. Population distributions of single-cell adhesion parameters during the cell cycle from high-throughput robotic fluidic force microscopy. *Sci. Rep.* **2022**, *12* (1), 7747.
(31) Cao, W.; Alsharif, N.; Huang, Z.; White, A. E.; Wang, Y.; Brown, K. A. Massively parallel cantilever-free atomic force microscopy. *Nat. Commun.* **2021**, *12* (1), 393.
(32) Gissibl, T.; Thiele, S.; Herkommer, A.; Giessen, H. Two-photon direct laser writing of ultracompact multi-lens objectives. *Nat. Photonics* **2016**, *10* (8), 554−560.
(33) Tu, D.; Tang, Y.; Huang, Y.; Tang, M.; Li, L.; Li, Y.; Lu, M.; Luo, Z.; Duan, Y. Next-Generation Wearable/Implanted Sensors Based on Fiber Optic and Its Application: From in Vitro to in Vivo. *ACS Sens.* **2025**, *10* (6), 3818−3839.
(34) Huang, J.; Albero Blanquer, L.; Bonefacino, J.; Logan, E. R.; Alves Dalla Corte, D.; Delacourt, C.; Gallant, B. M.; Boles, S. T.; Dahn, J. R.; Tam, H. Y.; Tarascon, J. M. Operando decoding of chemical and thermal events in commercial Na(Li)-ion cells via optical sensors. *Nat. Energy* **2020**, *5* (9), 674−683.
(35) Huang, H.; Liao, C.; Zou, M.; Liu, D.; Liu, S.; Wang, Y.; Bai, Z.; Liu, D.; Li, B.; Huang, J.; Wang, F.; Zhou, J.; Zhao, C.; Weng, X.; Liu, L.; Qu, J.; Wang, Y. Four-Dimensional Printing of a Fiber-Tip Multimaterial Microcantilever as a Magnetic Field Sensor. *ACS Photonics* **2023**, *10* (6), 1916−1924.
(36) Gonzalez-Hernandez, D.; Varapnickas, S.; Bertoncini, A.; Liberale, C.; Malinauskas, M. Micro-Optics 3D Printed via Multi-Photon Laser Lithography. *Adv. Opt. Mater.* **2023**, *11* (1), No. 2201701.
(37) Huang, H.; Zhu, D.; Wang, Y.; Liu, D.; Bao, W.; Chai, B.; Zhang, L.; Wang, Y.; Liao, C. Cr(VI)-Responsive Ink with Four-Dimensional Printing of an Ultracompact Hydrogel Optical Fiber Microsensor. *ACS sensors* **2025**, *10* (4), 2743−250.
(38) Xu, L.; Xue, Y.; Wang, C.; Gui, X.; Zhang, C.; Zhang, L.; Tao, Y.; Wang, X.; Zhang, L.; Pan, D.; Li, J.; Wu, D.; Chu, J.; Hu, Y. Hybrid Femtosecond Laser 3D Processing Technology for Rapid Integration of Functional Optical Devices on Fibers. *Laser Photonics Rev.* **2025**, *19* (7), No. 2400708.
(39) Zou, H.; Wu, S.; Shen, J. Polymer/silica nanocomposites: preparation, characterization, properties, and applications. *Chem. Rev.* **2008**, *100* (9), 3893−3957.
(40) Zou, M.; Liao, C.; Chen, Y.; Xu, L.; Tang, S.; Xu, G.; Ma, K.; Zhou, J.; Cai, Z.; Li, B.; et al. 3D printed fiber-optic nanomechanical bioprobe. *Int. J. Extreme Manuf.* **2023**, *5* (1), No. 015005.
(41) Shang, X.; Wang, N.; Cao, S.; Chen, H.; Fan, D.; Zhou, N.; Qiu, M. Fiber-Integrated Force Sensor using 3D Printed Spring-Composed Fabry-Perot Cavities with a High Precision Down to Tens of Piconewton. *Adv. Mater.* **2024**, *36* (2), No. 2305121.
(42) Xiong, C.; Zhou, J.; Liao, C.; Zhu, M.; Wang, Y.; Liu, S.; Li, C.; Zhang, Y.; Zhao, Y.; Gan, Z.; et al. Fiber-Tip Polymer Microcantilever for Fast and Highly Sensitive Hydrogen Measurement. *ACS Appl. Mater. Interfaces* **2020**, *12* (29), 33163−33172.
(43) Nejati, K.; Dadashpour, M.; Gharibi, T.; Mellatyar, H.; Akbarzadeh, A. Biomedical Applications of Functionalized Gold Nanoparticles: A Review. *J. Cluster Sci.* **2022**, *33* (1), 1−16.
(44) Zou, M.; Liao, C.; Liu, S.; Xiong, C.; Zhao, C.; Zhao, J.; Gan, Z.; Chen, Y.; Yang, K.; Liu, D.; Wang, Y.; Wang, Y. Fiber-tip polymer clamped-beam probe for high-sensitivity nanoforce measurements. *Light: Sci. Appl.* **2021**, *10* (1), 171.
(45) Li, R.; Ye, H.; Zhang, W.; Ma, G.; Su, Y. An analytic model for accurate spring constant calibration of rectangular atomic force microscope cantilevers. *Sci. Rep.* **2015**, *5*, 15828.
(46) Liao, C.; Xiong, C.; Zhao, J.; Zou, M.; Zhao, Y.; Li, B.; Ji, P.; Cai, Z.; Gan, Z.; Wang, Y.; Wang, Y. Design and realization of 3D printed fiber-tip microcantilever probes applied to hydrogen sensing. *Light: Adv. Manuf.* **2022**, *3* (1), 3−13.
(47) Ying, Z. C.; Reitsma, M. G.; Gates, R. S. Direct measurement of cantilever spring constants and correction for cantilever irregularities using an instrumented indenter. *Rev. Sci. Instrum.* **2007**, *78* (6), 2651.
(48) Chavan, D.; van de Watering, T. C.; Gruca, G.; Rector, J. H.; Heeck, K.; Slaman, M.; Iannuzzi, D. Ferrule-top nanoindenter: An optomechanical fiber sensor for nanoindentation. *Rev. Sci. Instrum.* **2012**, *83* (11), 115110.
(49) Liu, Q.; Xing, L.; Wu, Z.; Cai, L.; Zhang, Z.; Zhao, J. High-sensitivity photonic crystal fiber force sensor based on Sagnac interferometer for weighing. *Opt. Laser Technol.* **2020**, *123*, No. 105939.
(50) Li, D. M.; Feng, Y. M. Signaling mechanism of cell adhesion molecules in breast cancer metastasis: potential therapeutic targets. *Breast Cancer Research and Treatment* **2011**, *128* (1), 7.
(51) Wu, Y.; Liu, H.; Sun, Z.; Liu, J.; Li, K.; Fan, R.; Dai, F.; Tang, H.; Hou, Q.; Li, J.; Tang, X. The adhesion-GPCR ADGRF5 fuels breast cancer progression by suppressing the MMP8-mediated antitumorigenic effects. *Cell Death Dis.* **2024**, *15* (6), 455.
(52) Stefano, P.; Luigi, D. B.; Lucia, S.; Simona, C. Transmembrane Peptides as Sensors of the Membrane Physical State. *Front. Phys.* **2018**, *6*, 48.

https://doi.org/10.1021/acssensors.5c02849
ACS Sens. 2025, 10, 8874−8884

(53) Chaudhuri, O.; Cooper-White, J.; Janmey, P. A.; Mooney, D. J.; Shenoy, V. B. Effects of extracellular matrix viscoelasticity on cellular behaviour. *Nature* **2020**, *584* (7822), 535−546.
(54) Li, J.; Han, D.; Zhao, Y. P. Kinetic behaviour of the cells touching substrate: the interfacial stiffness guides cell spreading. *Sci. Rep.* **2014**, *4* (1), 3910.
(55) Zhou, C.; Wang, Q.; Zhang, D.; Cai, L.; Du, W.; Xie, J. Compliant substratum modulates vinculin expression in focal adhesion plaques in skeletal cells. *Int. J. Oral Sci.* **2019**, *11* (2), 18.
(56) Yang, M. T.; Sniadecki, N. J.; Chen, C. S. Geometric Considerations of Micro- to Nanoscale Elastomeric Post Arrays to Study Cellular Traction Forces. *Adv. Mater.* **2007**, *19* (20), 3119−3123.
(57) Shinde, A.; Illath, K.; Gupta, P.; Shinde, P.; Lim, K. T.; Nagai, M.; Santra, T. S. A Review of Single-Cell Adhesion Force Kinetics and Applications. *Cells* **2021**, *10* (3), 577.
(58) Ferrie, A. M.; Deichmann, O. D.; Wu, Q.; Fang, Y. High resolution resonant waveguide grating imager for cell cluster analysis under physiological condition. *Appl. Phys. Lett.* **2012**, *100* (22), 223701.
(59) Ungai-Salánki, R.; Peter, B.; Gerecsei, T.; Orgovan, N.; Horvath, R.; Szabó, B. A practical review on the measurement tools for cellular adhesion force. *Adv. Colloid Interface Sci.* **2019**, *269*, 309−333.
(60) Gerecsei, T.; Chrenkó, P.; Kanyo, N.; Péter, B.; Bonyár, A.; Székács, I.; Szabo, B.; Horvath, R. Dissociation constant of integrin-RGD binding in live cells from automated micropipette and label-free optical data. *Biosensors* **2021**, *11* (2), 32.
(61) Weder, G.; Vörös, J.; Giazzon, M.; Matthey, N.; Heinzelmann, H.; Liley, M. Measuring cell adhesion forces during the cell cycle by force spectroscopy. *Biointerphases* **2009**, *4* (2), 27−34.
(62) Vianay, B.; Senger, F.; Alamos, S.; Anjur-Dietrich, M.; Bearce, E.; Cheeseman, B.; Lee, L.; Théry, M. Variation in traction forces during cell cycle progression. *Biol. Cell* **2018**, *110* (4), 91−96.
(63) Panagiotakopoulou, M.; Lendenmann, T.; Pramotton, F. M.; Giampietro, C.; Stefopoulos, G.; Poulikakos, D.; Ferrari, A. Cell cycle−dependent force transmission in cancer cells. *Mol. Biol. Cell* **2018**, *29* (21), 2528−2539.

https://doi.org/10.1021/acssensors.5c02849
ACS Sens. 2025, 10, 8874−8884